Evolution of the shock front and turbulence structures in the shock/turbulence interaction

By N. Kevlahan[1], K. Mahesh[2] AND S. Lee[3]

The interaction of a weak shock front with isotropic turbulence has been investigated using Direct Numerical Simulation (DNS). Two problems were considered: the ability of the field equation (the equation for a propagating surface) to model the shock and a quantitative study of the evolution of turbulence structure using the database generated by Lee *et al.* (1992).

Field equation model predictions for front shape have been compared with DNS results; good agreement is found for shock wave interaction with $2D$ turbulence and for a single steady vorticity wave. In the interaction of $3D$ isotropic turbulence with a normal shock, strong alignment of vorticity with the intermediate eigenvector of the rate of strain tensor ($S^*_{ij} = S_{ij} - 1/3\delta_{ij}S_{kk}$) is seen to develop upstream of the shock and to be further amplified on passage through the shock. Vorticity tends to align at 90° to the largest eigenvector, but there is no preferred alignment with the smallest eigenvector. Upstream of the shock, the alignments continue to develop even after the velocity derivative skewness saturates. There is a significant tendency, which increases with time throughout the computational domain, for velocity to align with vorticity. The alignment between velocity and vorticity is strongest in eddy regions and weakest in convergence regions.

1. Introduction

The subject of this investigation is the interaction of a weak shock (mean upstream Mach number, $M_1 = 1.05 - 1.20$) with relatively strong turbulence ($M_t = 0.07 - 0.40$ where M_t is the fluctuation Mach number defined as $q/\bar{c}$; q is a velocity scale of the turbulence and $\bar{c}$ is the mean sound speed). The interaction of shock waves with turbulence has been studied analytically (using the Linear Interaction Analysis) by many authors (eg. Ribner 1954, McKenzie & Westphal 1968, Anyiwo & Bushnell 1982). Experimental investigations have recently been carried out by Jacquin *et al.* (1991), Honkan & Andreopoulos (1990) and Hesselink & Sturtevant (1988). Numerical simulations of the shock turbulence interaction have been performed by Rotman (1991) and Lee *et al.*(1992).

We study shock/turbulence interaction as simulated by Lee *et al.* (1992). In the simulation the reference frame is fixed with respect to the mean shock position; the mean flow approaches the shock supersonically ($M_1 > 1$) and exits subsonically. Shock wave structure is resolved by the Navier-Stokes equations without

1 University of Cambridge
2 Stanford University
3 Center for Turbulence Research

using shock-fitting or shock-capturing techniques. Inflow turbulence is generated with a prescribed energy spectrum ($E(k) \propto k^4 \exp(-k^2)$) and is then allowed to evolve naturally as the flow approaches the shock front. The turbulence should be fully developed by the time it reaches the shock wave, and this is verified by making sure that the velocity derivative skewness stabilizes well upstream of the shock. Pressure and density are kept constant in the inflow plane. The simulation uses a $193 \times 64 \times 64$ grid and the Reynolds number based on the Taylor microscale, Re_λ, is 16.7.0. The study is divided into two parts: the effect of the turbulence on the shock (shock front evolution), and the effect of the shock on the turbulence (turbulence structure evolution).

In the first part of this study we test a new model for shock front/turbulence interaction based on a field equation approach where the front is treated as a surface which propagates normal to itself and is distorted by the turbulent velocity field. This model not only gives the instantaneous position and shape of the front, but can also be used to close the Rankine-Hugoniot equations for a curved front. Once the Rankine-Hugoniot equations have been closed, the turbulence quantities downstream of the shock can be calculated. In the weak shock/relatively strong turbulence regime considered here, the shock may become significantly distorted (however, it will still remain identifiable). Because of this strong deformation, the evolution of the shock front will not be well predicted by linear theories such as the Linear Interaction Analysis (LIA) which assume that the shock merely copies the shape of the distorting velocity field but at a different amplitude. The field equation, being nonlinear, can be used in such cases of large shock front distortion. The field equation approach has the advantages of simplicity and ease of numerical implementation. One important practical application of the field equation approach would be its inclusion in DNS to avoid having to numerically resolve the shock wave structure. Removing this restriction would greatly increase the maximum Mach number that can be reached using DNS. The field equation model is validated by comparing the shape and position of the shock front predicted by the field equation with two-dimensional DNS results under the same conditions. The field equation model is described in more detail in §2 below.

The second part of this investigation is a quantitative study of turbulence structure evolution. In this part, we analyze turbulence structure in planes (parallel to the mean shock) upstream and downstream of the shock. We are interested both in general aspects of turbulence structure and its development and in the effect of the rapid compression on the turbulence structure as it passes through the shock. To characterize turbulence structure we consider three dynamically important properties of the flow: (i) the angle between the vorticity and the shock normal, (ii) the angle between the vorticity and the eigenvectors of the strain rate tensor, (iii) the angle between the velocity and vorticity vectors. The flow is also divided into four classes of structure (eddies, shear, convergence, and streaming) based on local values of the rate of strain and rate of rotation tensors. Since we are interested in turbulence evolution, in all cases the instantaneous mean (computed by averaging over homogeneous directions) is subtracted before any analysis is performed.

2. Modeling shock front evolution

2.1. The field equation model

In this section we describe the validation of the field equation model applied to shock/turbulence interaction by comparison with DNS.

The field or G-equation model has been introduced by Kerstein *et al.* (1988) as a model for the propagation of a zero-thickness, constant-density premixed flame through a homogeneous turbulent flow. In this model a continuous scalar $G(x,y,t) = x - g(x,y,t)$ is convected by the flow with the surface $G(x,y,t) = 0$ corresponding to the position of the physical flame front. The flame propagates at a speed u_F normal to itself and is at the same time advected by the turbulent flow (u) as described by equation (1) below.

$$\frac{\partial G}{\partial t} + \mathbf{u} \cdot \nabla G = u_F |\nabla G| \tag{1}$$

In general, u_F will be a function of the shape of the front, the local straining, and the history of the distortion (in the case of the flame front u_F is modeled as a function of local strain and curvature—the flame stretch).

The aim of this study is to determine whether the field equation model can be usefully applied to the propagation of a shock front through a turbulent flow. Initially, we take the simplest two-dimensional form of the model where u_F is taken as a constant: the laminar propagation speed of the front. If it is assumed that the front does not curl over on itself (as is assumed in the usual derivation of the Rankine-Hugoniot conditions for a curved front), then equation (1) for the propagation of the front may be re-written in terms of $g(y,t)$ as

$$\frac{\partial g}{\partial t} = u_F(1 + g_y^2)^{1/2} + u - v g_y \tag{2}$$

where u and v are, respectively, the x- and y-components of the turbulent velocity field (in a frame fixed in the mean shock, the mean shock speed must be subtracted from u), and the initial condition is that $g(y,0) = 0$. Once equation (2) has been solved, $g_t(y,t)$ and $g_y(y,t)$ may be substituted into the Rankine-Hugoniot equations for a curved shock,

$$g_t[\rho] + g_y[\rho V] = [\rho U] \tag{3a}$$

$$g_t[\rho U] + g_y[\rho UV] = [\rho U^2 + P] \tag{3b}$$

$$g_t[\rho V] + g_y[\rho V^2 + P] = [\rho UV] \tag{3c}$$

$$g_t[\rho E] + g_y[V(\rho E + P)] = [U(\rho E + P)] \tag{3d}$$

to obtain the changes of turbulence quantities downstream of the shock front. In equations (3a-d), [ ] indicates the difference of the quantity in the brackets across the front and E is the internal energy ($= P/(\gamma - 1) + (U^2 + V^2)/2$ for an ideal gas). Equations 3(a-d) represent, respectively, conservation of mass, x–momentum,

$y-$momentum, and total energy across the shock front. The above conditions can be combined to give a further condition: the tangential component of velocity is continuous across the front. Equations (3a-d) can be solved for the turbulence (fluctuating) quantities u_2, v_2, P_2, and ρ_2 downstream of the shock in terms of $g_t(y,t)$ and $g_y(y,t)$ and the upstream quantities:

$$\begin{aligned} u_2 =&\{g_y^3(\gamma+1)u_1v_1 + g_y^2[2v_1^2 - (\gamma+1)u_1^2 + (\gamma+1)u_1g_t - 2\gamma P_1/\rho_1] + \\ & g_y[(\gamma-3)u_1v_1 + 4v_1g_t] + (1-\gamma)u_1^2 + (\gamma-3)u_1g_t - 2\gamma P_1/\rho_1 + 2g_t^2\}/ \\ & \{(\gamma+1)[g_y^3v_1 + (1+g_y^2)(g_t-u_1) + g_yv_1]\} \end{aligned} \tag{4a}$$

$$v_2 = v_1 + g_y(u_1 - u_2) \tag{4b}$$

$$P_2 = P_1 + \rho_1[u_1^2 - g_yu_1v_1 - g_tu_1 + u_2(g_yv_1 + g_t - u_1)] \tag{4c}$$

$$\rho_2 = \frac{\rho_1(g_yv_1 + g_t - u_1)}{[g_y^2u_1 + g_yv_1 + g_t - u_2(1+g_y^2)]} \tag{4d}$$

Note that equations (4a-d) are *exact* solutions for the downstream quantities; no approximations or additional assumptions have been made in their derivation.

So we see that the field equation model for shock front evolution (2) provides a nonlinear closure to the Rankine-Hugoniot equations for a curved shock (3a-d) which allows us to obtain the changes in turbulence quantities across the shock (equations 4a-d). Because the closure is nonlinear and because we have made no linearizing assumptions in solving the Rankine-Hugoniot equations, this field equation/Rankine-Hugoniot model will be able to treat large deformations of the shock front and to predict nonlinear amplifications effects of turbulence quantities across the front. LIA theory cannot be applied in the case of large deformation and will not be able to predict any nonlinear amplification. Shock dynamics theory is mathematically complicated and awkward to use in the case of fully developed turbulence.

The assumption of constant u_F is in a sense equivalent to the geometrical acoustics limit of shock dynamics. In both cases, the rays of an initially curved front in a uniform flow (eg. in the shock focusing experiments of Sturtevant & Kulkarny (1976)) will eventually cross, leading to a cusp-shaped front. The field equation (2) for the propagation of the front is not, however, the same as the eikonal equation for geometrical acoustics: $g_t^2 = c^2g_y^2$. That the field equation model is a better physical model than the eikonal equation for geometrical acoustics can be seen by working out the second order perturbation solution to the exact Rankine-Hugoniot equations (3a-d) for the evolution of the shock front.

The Rankine-Hugoniot equations for a curved front may be closed to second order by assuming that the flow downstream of the front is isentropic. The assumption of isentropy is very good for weak shocks: changes in entropy are of third order in the pressure jump across the shock. This leads to the following relation between pressure and density fluctuations:

$$p = \gamma\frac{P}{R}\rho\left(1 + \frac{1}{2}(\gamma-1)\frac{\rho}{R}\right), \tag{5}$$

where upper case indicates mean quantities and lower case indicates fluctuating quantities. Combining equations (3a-d) with equation (5) closes the Rankine-Hugoniot equations to second order. Performing a perturbation expansion to second order in the $O(\epsilon)$ quantities u, v, P, ρ, g_t, and g_y on finds the following second-order solution for the evolution of the shock front:

$$g_t^2 + g_t(F_1 - 2u_1) = F_1 u_1 - u_1^2 + F_2 g_y v_1 + F_3 g_y^2 \tag{6}$$

where the F_i's are coefficients that depend on mean flow quantities. From equation (5), letting $g_t = \epsilon g_{1t} + \epsilon^2 g_{2t} + O(\epsilon^3)$, $g_y = \epsilon g_{1y} + \epsilon^2 g_{2y} + O(\epsilon^3)$, $u_1 = \epsilon u_1$, $v_1 = \epsilon v_1$ the first-order solution is

$$g_{1t} = u_1, \tag{7}$$

and the second-order solution is

$$g_{2t} = \frac{F_3}{F_1} g_{1y}^2 + \frac{F_2}{F_1} g_{1y} v_1. \tag{8}$$

Now, a similar second-order perturbation expansion for the field equation (2) yields the following solutions:

$$g_{1t} = u_1 \tag{9}$$

and,

$$g_{2t} = \frac{1}{2} u_F g_{1y}^2 - g_{1y} v_1. \tag{10}$$

Thus, we see that the field equation gives essentially the same behavior as the solution of the full Rankine-Hugoniot equations, at least to second order. Note that the Rankine-Hugoniot equations do not have a closed-form analytical solution.

Nonlinear shock dynamics theory allows the shock propagation velocity to vary in proportion to the inverse square root of ray tube areas. This leads to higher propagation speeds in concave regions and lower speeds in convex regions of the front, thus reducing the tendency to form cusp. The assumption of constant u_F should be good until the constant u_F equation predicts cusp formation. In practice, when the front is distorted by a turbulent flow it will never distort to the extent of forming cusps, so the assumption of constant u_F is well justified. In the case of very weak shocks/strong turbulence, some variation of u_F (perhaps a dependence on shock curvature) should be included in the model.

2.2. Validating the field equation model

The field equation model is validated by comparing its predictions of front evolution with DNS. Since our interest is in nearly incompressible turbulence interacting with the shock, we consider the interaction of vorticity waves with the shock. Three cases are considered in order of increasing complexity (see Figure 1). First, the interaction of a shock with a single steady vorticity wave (one sine wave $u = A \sin ky$ at normal incidence to the shock), next, the interaction of a shock with a single

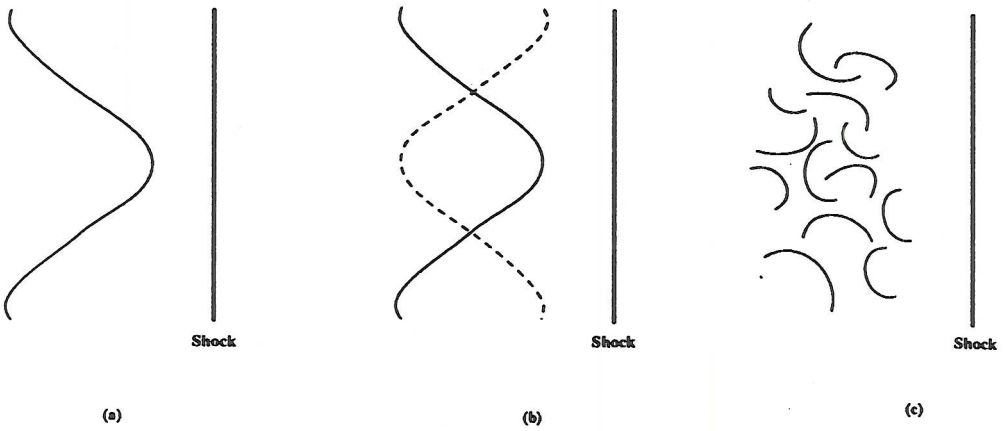

FIGURE 1. The three cases considered. (a) Steady, single mode, $u = A \sin ky$, (b) unsteady, single mode, $u = A \sin ky \cos \omega t$. $\tau_{\text{turb.}}/\tau_{\text{shock}} \sim 1$, (c) unsteady, many modes, 'full turbulence'. $\tau_{\text{turb.}}/\tau_{\text{shock}} \gg 1$.

unsteady mode, and finally, the interaction of a shock with $2D$ turbulence (many unsteady modes at various angles of incidence).

In the second case, the time for the shock to pass through the 'turbulence' is of the same order as the time-scale of the 'turbulence', while in the third case, the time for the shock to pass through an eddy is much less than the turnover time of the eddy.

In the first case, the prediction of the field equation is calculated from its third-order perturbation expansion solution:

$$\begin{aligned}\phi(\eta,\tau) =& \tau + \epsilon\tau \sin\eta + \frac{1}{6}\epsilon^2\tau^3 \cos^2\eta \\ &- \frac{1}{15}\epsilon^3\tau^5 \sin\eta \cos^2\eta + O(\epsilon^4).\end{aligned} \tag{11}$$

Where non-dimensional quantities $\epsilon = u/u_F$, $\eta = ky$, $\tau = u_F tk$, $\phi = kg$. Note that a *secularity* in time appears in (11): the perturbation expansion will break down when

$$\tau_c = \epsilon^{-1/2} \tag{12}$$

or,

$$t_c = (k^2 u_F u)^{-1/2}. \tag{13}$$

This is the time one expects the front to form *cusps* (places where the curvature becomes infinite). The simple version of the field equation with constant u_F is valid until t_c.

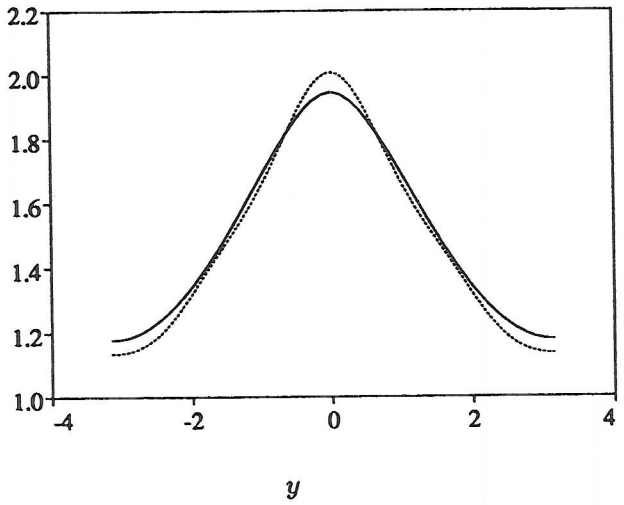

FIGURE 2. Comparison of front shape in DNS with field equation prediction. Comparison is made just before cusp formation (the worst time of agreement). —— DNS, ---- Field equation

For the second case, the field equation is solved numerically using a Fourier spectral method; for the third case, the field equation with a viscous term $\epsilon\nabla^2 G$ for numerical stability is incorporated into the code of Lee *et al.* (1992). In all three cases, the position of the shock in the DNS is found from the pressure half-rise point.

In the first case, the agreement between the field equation and DNS was very good until the time predicted by the field equation for cusp formation. Both the curvature and front shape agreed well (see Figure 2). After the 'cusp' formed the DNS showed the formation of two secondary shocks which increased in strength and extent over time, while the original shock decreased in strength (see Figure 3). The post-cusp multi-shock DNS results are similar to what was seen in the shock-focusing experiments of Sturtevant & Kulkarny (1976).

The agreement in the second case is very poor: both the shape and magnitude of the distortion predicted by the field equation do not match the DNS results. We believe this discrepancy is due to the larger deviation of u_F from its assumed constant value in this case.

In the case of $2D$ turbulence ($M_1 = 1.2, M_t = 0.07$), the agreement of the field equation prediction with DNS is very good, even over periods as long as three eddy turnover times ($\tau_{turb.} = \lambda/u'$). The correlation between the displacement and slope of the field equation predictions and DNS is always over 80%, and mostly above 90% (see Figure 4). The RMS error of the field equation predictions for displacement and slope are also relatively low: generally less than 50% (see Figure 4). The fact that the field equation model works well in the case of turbulence and the steady vorticity wave, but not for the unsteady wave, indicates that the shock sees the turbulence as

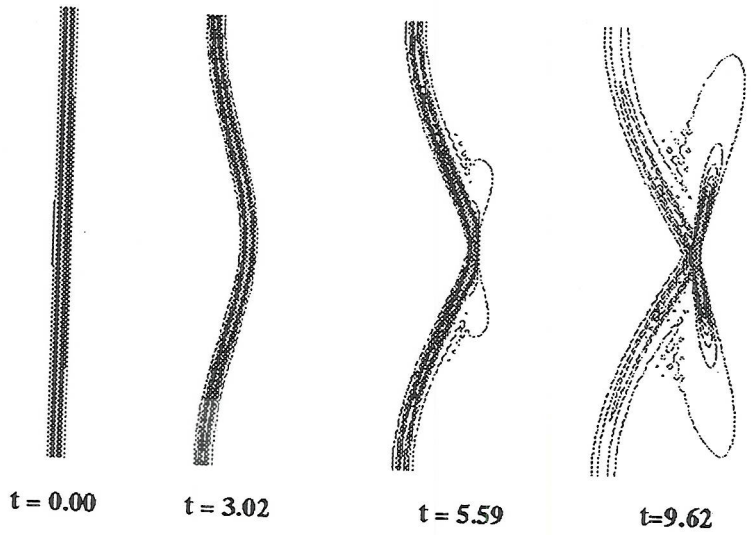

FIGURE 3. Evolution of front shape in DNS. Quantity plotted is dilatation. Note the cusp-like shape at t=5.59 and the formation of strong secondary shocks by t=9.62

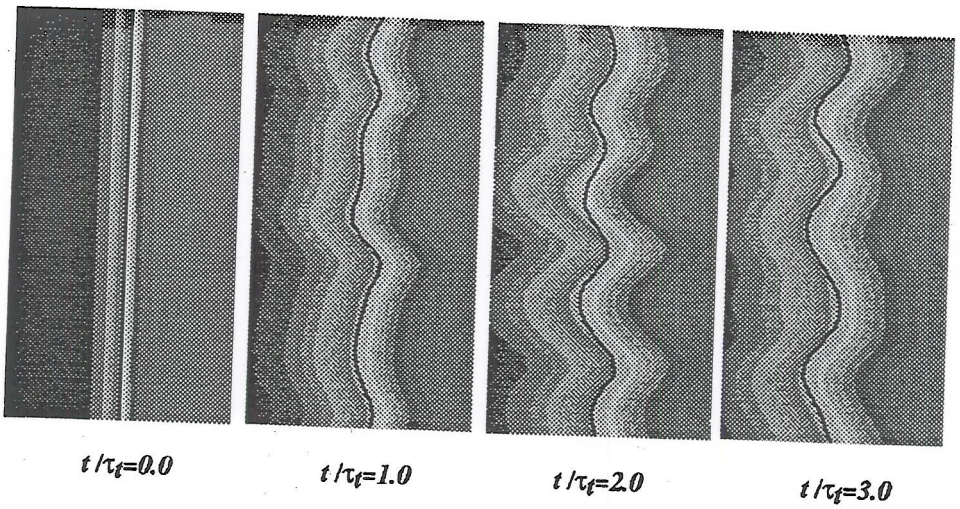

FIGURE 4. Comparison between instantaneous shock position in DNS and field equation prediction over time. The dark line is the DNS prediction.

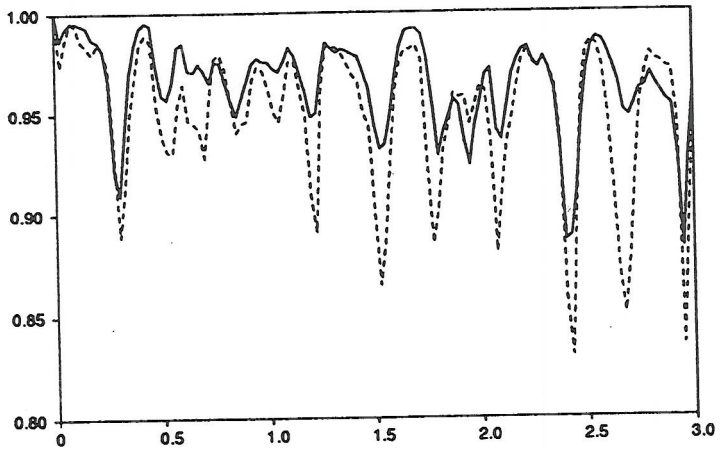

FIGURE 5A. Correlation between DNS and field equation of instantaneous shock position in 2D shock/turbulence interaction —— Displacement, ---- Slope

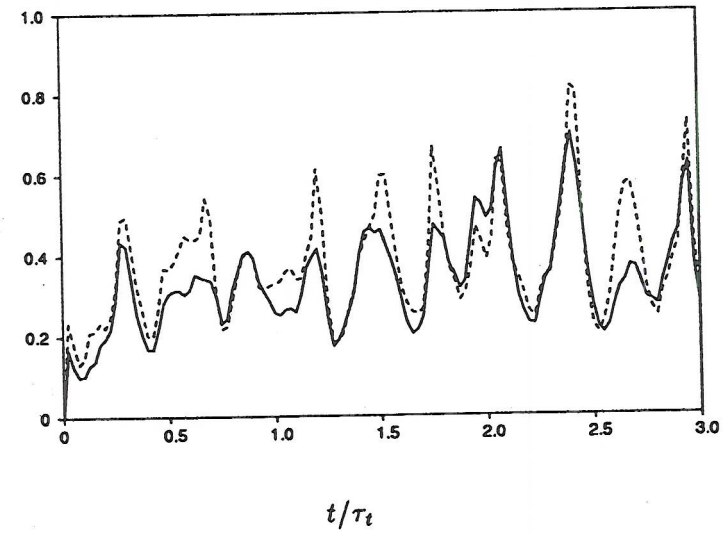

FIGURE 5B. RMS error in the field equation prediction of instantaneous shock position in 2D shock/turbulence interaction —— Displacement, ---- Slope

frozen. Hence, the case of turbulence corresponds to the steady case (the turbulence time scale is about 1/100 the shock passage time) and the agreement of the field equation model with DNS is good. Note that presence of multiple modes at various angles of incidence does not seem to affect the validity of the field equation model.

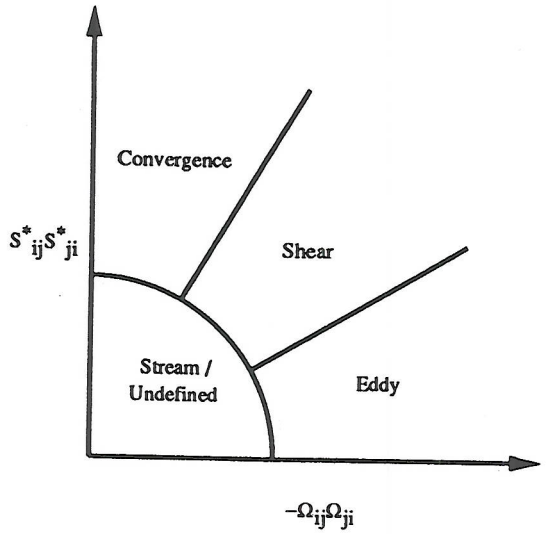

FIGURE 6. Schematic of the way the $S^*_{ij}S^*_{ji}$- $-\Omega_{ij}\Omega_{ji}$ plane is divided into four characteristic structures.

3. Evolution of turbulence structure

In this section, we use the database of Lee *et al.* (1992) to study the evolution of turbulence structure in $3D$ isotropic turbulence/normal shock interaction. The results presented correspond to case C for which $M_1 = 1.2$, $M_t = 0.095$, and $Re_\lambda = 11.9$ upstream of the shock. The following three quantities were investigated: (i) the angle between the vorticity vector (ω) and the shock-normal, (ii) the angle between ω and the eigenvectors of the trace-free strain rate tensor defined as,

$$S^*_{ij} = \frac{1}{2}\left(\frac{\partial u_i}{\partial x_j} + \frac{\partial u_j}{\partial x_i}\right) - \frac{1}{3}\delta_{ij}\frac{\partial u_k}{\partial x_k}, \tag{14}$$

and (iii) the angle between the velocity and vorticity vectors.

The angle between ω and the eigenvectors of the rate of strain is indicative of the type of turbulence structure. Recent DNS of homogeneous, isotropic turbulence (eg. Ashurst *et al.* 1987, Vincent & Meneguzzi 1991) show that the vorticity vector aligns with the *intermediate* eigenvector of the strain rate tensor. The angle between the velocity and vorticity gives the balance between helicity density (their dot product, believed to be related to coherent large scale structures) and the nonlinear transfer of energy between scales (a function of their cross product). Some DNS (eg. Pelz *et al.* 1985 and She *et al.* 1991) show a tendency for the velocity and vorticity to align (a reduction in nonlinearity), while others (eg. Rogers & Moin 1987) see little preferential alignment.

We also compute the ratio of eigenvalues of S^*_{ij} $(\alpha : \beta : \gamma)$ and the relative numbers of 'cigar' $(\alpha\beta\gamma > 0)$ and 'pancake' $(\alpha\beta\gamma < 0)$ regions (see Kevlahan (1992). In addition, we classify the flow (see Figure 6) into four structures (convergence, shear, eddy, and streaming) based on $(S^*_{ij}S^*_{ji})$ and the $(-\Omega_{ij}\Omega_{ji})$ (where Ω_{ij} is the rotation

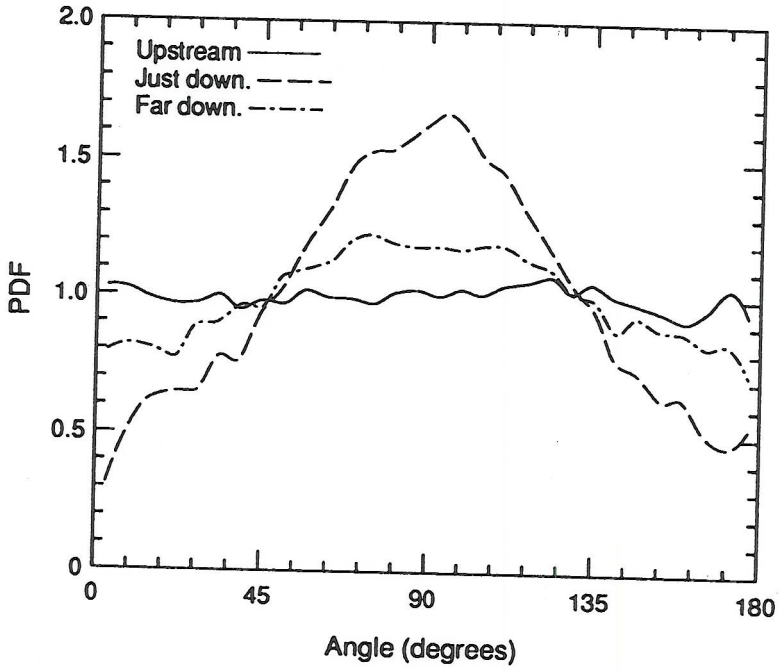

FIGURE 7. PDF of the angle between vorticity and the shock normal upstream of the shock (plane 72), just downstream of the shock (plane 111), far downstream (plane 174). The PDFs have been normalized by dividing by the sine of the angle and scaled so that 1.0 corresponds to a flat distribution. Note the persistence of the alignment far downstream where the flow is essentially incompressible.

rate tensor). Structures are further classified as incompressible, compressed, or expanded based on the value of $S_{kk}^2/(S^{*^2} + \Omega^2)$ (if greater than 5% the region is classified as compressible) and S_{kk} (less than zero, compressed; greater than zero, expanded).

According to this structural classification, convergence regions are places of high irrotational straining, shear regions are places of approximately equal rotational and irrotational straining, eddies are regions of high rotational straining, and stream regions are places where both the rotational and irrotational strains are small but the kinetic energy is large.

The quantities described above are calculated in planes parallel to the mean shock and averaged over ten realizations and homogeneous directions. The instantaneous means over the plane are subtracted from each quantity before they are analyzed. This eliminates the mean flow distortion and allows us to concentrate on the behavior of the turbulence itself. The PDFs of angles are normalized by the sine of the angle so that vectors isotropically distributed will lead to a flat distribution (if vectors are distributed isotropically over a sphere then the number of vectors at any angle to the 'north pole' is proportional to the sine of the angle).

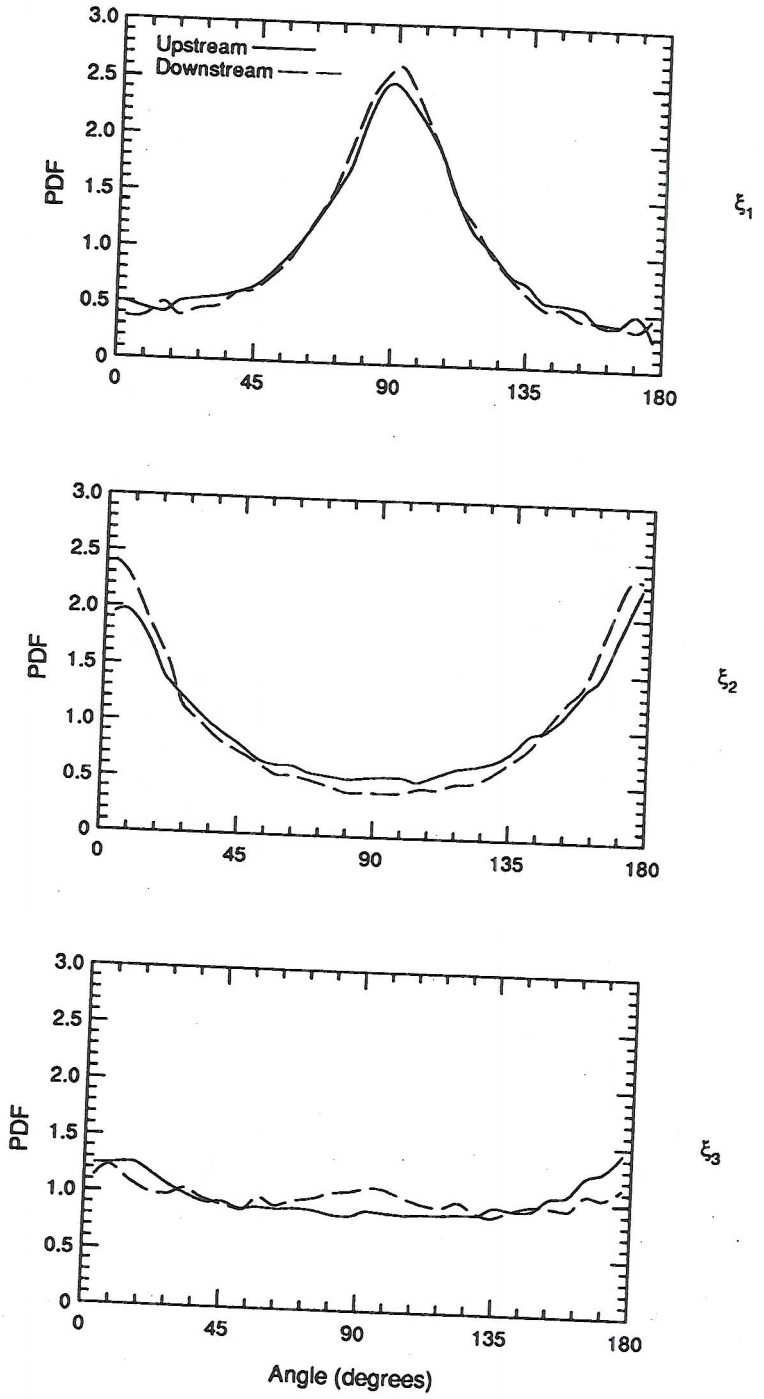

FIGURE 8. PDFs of the angle between the vorticity vector and the three eigenvectors of the rate of strain tensor upstream and downstream of the shock. Note the amplification of the alignments by the shock. The PDFs have been normalized by dividing by the sine of the angle and scaled so that 1.0 corresponds to a flat distribution. (a) Angle with largest eigenvector, (b) angle with middle eigenvector, (c) angle with smallest eigenvector.

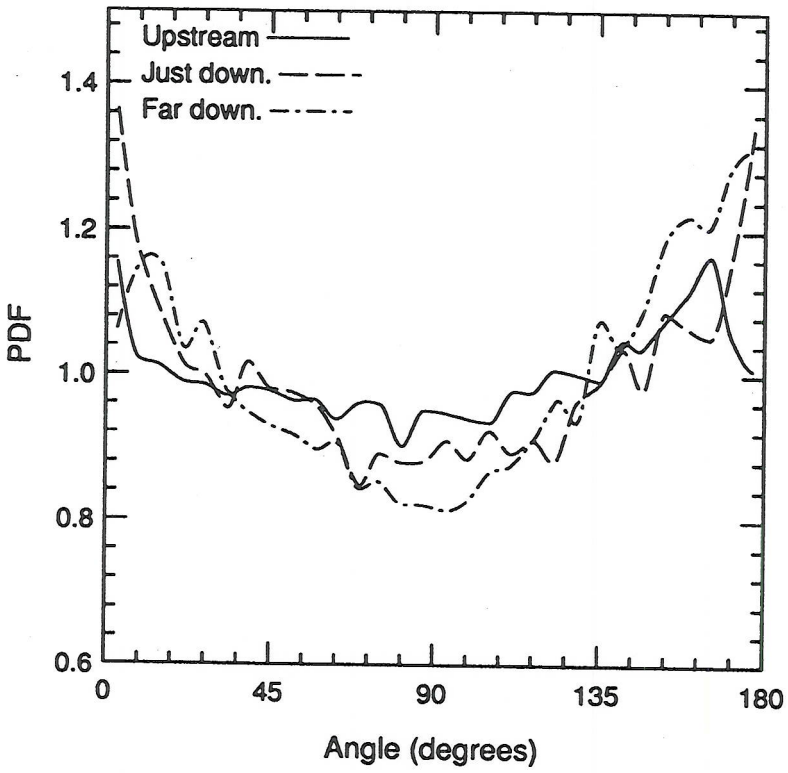

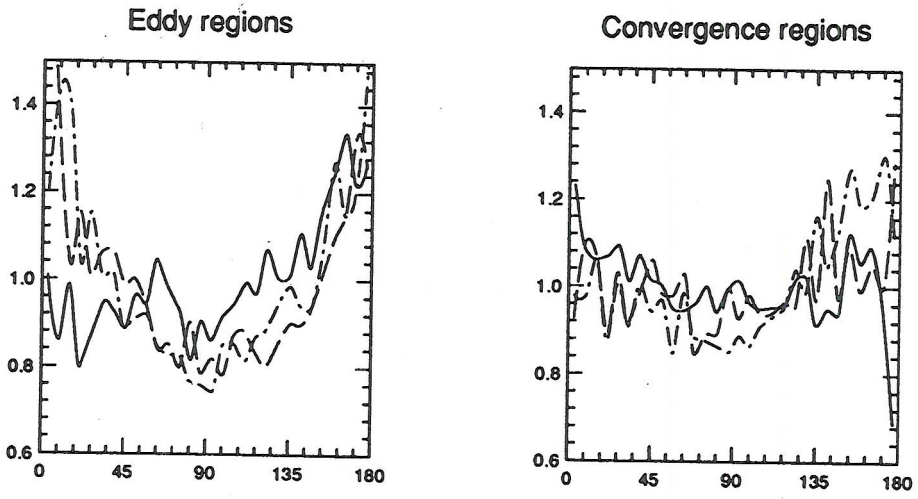

FIGURE 9. Angle between the vorticity and velocity vectors. Note the significant tendency for the vorticity and velocity vectors to align. (a) Overall, (b) in eddy regions, (c) in convergence regions.

3.1. Turbulence structure results

The eigenvalues of S^*_{ij} are in the ratio $4 : 1 : -5$ and are unchanged up and downstream of the shock except in the vicinity of the shock itself where the middle eigenvalue increases leading to the ratio $2 : 1 : -3$. These results are similar to the ratio $3 : 1 : -4$ found by Chen *et al.* (1990) for isotropic incompressible flows. The flow is divided into pancake and cigar regions in the ratio $3 : 1$ both upstream and downstream of the shock. The flow is composed of 27% convergence, 39% shear, 23% eddies, and 4% streams (7% undefined). This distribution is constant up and downstream of the shock. In the vicinity of the shock, the distribution changes to 33% convergence, 26% shear, 11% eddies, and 8% streams (22% undefined). In the vicinity of the shock, 82% of structures are compressible, and of these half are expanded and half are compressed. Eddies and shear regions are primarily *expanded* structures, while convergence regions are primarily *compressed*.

The vorticity vector preferentially aligns parallel to shock surface downstream of the shock with a probability 1.7 times as much as in a flat distribution (see Figure 7). This is a well known effect of the compression in the shock normal direction which amplifies the vorticity parallel to the shock and leaves vorticity normal to the shock unchanged.

Upstream of the shock where the turbulence is isotropic, we observe a very strong tendency for ω to align with ξ_2 (the middle eigenvector of S^*_{ij}) and to align at 90° to ξ_1 (the largest eigenvector of S^*_{ij}) (see Figure 8). Alignment of the vorticity with ξ_2 and at 90° to ξ_1 is 2.5 times more likely than in a flat distribution. The PDF of the angle between ω and ξ_3 is approximately flat. These alignments saturate before the turbulence interacts with the shock. The alignments are further amplified on passage through the shock, which is consistent with the Rapid Distortion Analysis of Kevlahan (1992). An interesting point regarding the flow upstream of the shock is that this alignment continues to develop *after* the velocity derivative skewness has saturated. This may suggest that skewness saturation may not be the best indicator that the turbulence is fully developed (evidently some structural evolution continues even after the skewness has stabilized).

We observe a significant tendency for the velocity and vorticity vectors to align (see Figure 9). This tendency increases as the flow moves through the computational domain. Alignment (or anti-alignment) far downstream is about 1.35 times as likely as in flat distribution. This alignment is strongest in eddy regions (1.48 times as likely) and weakest in convergence regions (about 1.05 times as likely). This indicates that the primary cause of the increase in helicity density (or decrease in nonlinearity) is vortical rather than irrotational straining. There also seems to be a tendency towards asymmetry upstream of the shock (eddies tend to antialign), although this may not be significant. These results are somewhat stronger than those of Rogers & Moin (1987) who find at most only a 20% deviation from a flat distribution. This discrepancy may be due to the differences in the flows (ours is slightly compressible and theirs is incompressible) or because our Reynolds number is relatively low (about 25) and they find that the reduction in nonlinearity decreases as Reynolds number increases.

4. Conclusions

Field equation model predictions for front shape have been compared with DNS results, and agreement is very good for $2D$ turbulence ($M_1^U = 1.20$, $M_t = 0.07$) and for a single steady vorticity wave. The field equation approach shows promise as a way of modeling the shock/turbulence interaction.

The eigenvalues of S_{ij}^* in the developed turbulence are in the ratio $4 : 1 : -5$, except in the vicinity of the shock where they are in the ratio $2 : 1 : -3$. The ratio of pancake to cigar type straining regions is in the ratio $3 : 1$.

In the vicinity of the shock, 82% of structures are compressible and of these half are expanded and half are compressed. Eddies and shear regions are primarily *expanded* structures, while convergence regions are primarily *compressed* downstream of the shock.

Strong alignment of vorticity with the intermediate eigenvector of the trace-free strain rate tensor is seen upstream of the shock and further amplifies on passage through the shock. Vorticity tends to align at 90° to the largest eigenvector, but there is no preferred alignment with the smallest eigenvector. The alignments continue to develop upstream even after the skewness saturates. This suggests that skewness may not be the best indicator of fully developed isotropic turbulence.

It is interesting to note that our results on the alignment of vorticity with ξ_2 and the ratio of the eigenvalues are sometimes thought to be the result of turbulent structures such as long vortex tubes (eg. Jiménez 1992), and yet our Reynolds number is too low for these tubes to have formed.

There is a significant tendency for velocity to align with vorticity. This tendency continues to increase with time throughout the computational domain. The alignment between velocity and vorticity is strongest in eddy regions and weakest in convergence regions.

REFERENCES

ANYIWO, J. C. & BUSHNELL, D. M. 1982 Turbulence amplification in shock-wave boundary-layer interaction. *AIAA J.* **20**(7), 893-899.

ASHURST, W. T., KERSTEIN, A. R., KERR, R. M. & GIBSON, C. H. 1987. Alignment of vorticity and scalar gradients with strain rate in simulated Navier-Stokes turbulence. *Phys. Fluids* **30**(8), 2343-2353.

CHEN, J. H., CHONG, M. S., SORIA, J., SONDERGAARD, R., PERRY, A. E., ROGERS, M., MOSER, R., & CANTWELL, B. J. 1990 A study of the topology of dissipating motions in direct numerical simulations of time-developing compressible and incompressible mixing layers. In *Studying turbulence using numerical simulation databases - III, Proceedings of the 1990 summer program.* Stanford: CTR.

HESSELINK, L. & STURTEVANT, B. 1988 Propagation of weak shocks through a random medium. *J. Fluid Mech.* **196**, 513-553.

HONKAN, A. & ANDREOPOULOS, J. 1990 Experiments in a shock wave/homogeneous turbulence interaction. *AIAA Paper*, No. 90-1647.

JACQUIN, L., BLIN, E. & GEFFROY, P. 1991 Experiments on free turbulence/ shock wave interaction. *Eighth Symposium on turbulent shear flows*, Munich, September 9-11, 1991.

JIMÉNEZ, J. 1992 Kinematic alignment effects in turbulent flows. *Phys. Fluids A.* 4(4), 652-654.

KERSTEIN, A. R., ASHURST, W. T. & WILLIAMS, F. A. 1988 Field equation for interface propagation in a unsteady homogeneous flow field. *Phys. Rev. A.* **37**, 2728.

KEVLAHAN, N. 1992 Rapid distortion of turbulent structures. In *Proceedings of the fourth European turbulence conference*. To appear.

LEE, S., MOIN, P., & LELE, S. K. 1992 The interaction of isotropic turbulence with a shock wave. *Report No. TF-52*. Thermosciences Division, Department of Mechanical Engineering, Stanford University.

MCKENZIE, J. F. & WESTPHAL, K. O. 1968 Interaction of linear waves with oblique shock waves. *Phys. Fluids.* **11(11)**, 2350-2362.

RIBNER, H. S. 1954 Convection of a pattern of vorticity through a shock wave.. *NACA TN-2864.*

ROGERS, M. M. & MOIN, P. 1987 Helicity fluctuations in incompressible turbulent flows. *Phys. Fluids* A. **30**(9), 2662-2671.

SHE, Z., JACKSON, E. & ORSZAG, S. A. 1991 Structure and dynamics of homogeneous turbulence: models and simulations. *Proc. R. Soc. Lond.* A. **434**, 101-124.

STURTEVANT, B. & KULKARNY, V. A. 1976 The focusing of weak shock waves. *J. Fluid Mech.* **73**(4), 651-671.

VINCENT, A. & MENEGUZZI, M. 1991 The spatial structure and statistical properties of homogeneous turbulence. *J. Fluid Mech.* **225**, 1-20.

WHITHAM, G. B. 1957 A new approach to problems of shock dynamics. Part I. Two-dimensional problems. *J. Fluid Mech.* **2**, 145-171.

ZANG, T. A. & BUSHNELL, D. M. 1984 Numerical computation of turbulence amplification in shock-wave interactions. *AIAA J.* **22**(1), 13-21.